Journal of Catalysis **191,** 218–224 (2000)
doi:10.1006/jcat.1999.2774, available online at http://www.idealibrary.com on IDEAL®

Characterization and Catalytic Activity of MCM-22 and MCM-56 Compared with ITQ-2

A. Corma,[1] U. Diaz, V. Fornés, J. M. Guil,* J. Martínez-Triguero, and E. J. Creyghton†

*Instituto de Tecnología Química (UPV-CSIC), Universidad Politécnica de Valencia, Avenida de los Naranjos, s/n, 46022 Valencia, Spain; *Instituto Química Física Rocasolano (CSIC), C/ Serrano 119, 28006 Madrid, Spain; and †Shell Research and Technology Center, Amsterdam, Badhuisweg 3, 1031 CM, Amsterdam, The Netherlands*
E-mail: acorma@itq.upv.es

Received September 15, 1999; revised November 26, 1999; accepted November 26, 1999

MCM-22, MCM-56 and ITQ-2 zeolites, have been characterized by different physicochemical techniques (XRD, ^{29}Si MAS NMR, IR, adsorption, and catalytic test), and they show that the first two are similar in structure and reactivity while ITQ-2 is different. The external surface area of the MCM-56 sample is somewhat larger than MCM-22, both being much smaller than ITQ-2. This is in agreement with the 15–20% larger adsorption capacity for 1,3,5-trimethylbenzene shown by MCM-56 with respect to MCM-22, and the seven times larger adsorption shown by ITQ-2. This is a consequence of a higher degree of disorder along the *c* axes in MCM-56 than in MCM-22. A similar type of disorder, i.e., the same XRD pattern than for MCM-56, was observed after adsorbing acetone on the laminar precursor of MCM-22. The external surface acidity of the three samples, as measured by 2,6 ditertbutylpyridine (26 DTBPy), follows the order ITQ-2 > MCM-56 > MCM-22 and this is reflected by the catalytic activity towards a large molecule (1,3,5-triisopropylbenzene) which can react only at the external surface (external cups) of these materials.

Key Words: **MWW-type zeolites; delaminated zeolites; role of external surface in zeolites.**

INTRODUCTION

MCM-22 (1) is one of the most interesting zeolite structures synthesized up to now. It consists of two independent pore systems, one formed by two-dimensional sinusoidal channels, and the other by large supercages having an inner diameter of approximately 0.71 nm and a height of 1.82 nm. Both channel systems are accessible through 10 member ring (MR) openings (2). Precedents of MCM-22 could be found in PSH-3 (3) and SSZ-25 (4) zeolites. In the case of PSH-3 and MCM-22 hexamethyleneimine was used as the directing agent, while SSZ-25 was synthesized from a reaction mixture containing 1,3,5-trimethyladamantylammonium ion and KOH. Later (5), it was shown that the structure could be more efficiently synthesized from a reaction mixture containing hexamethyleneimine and 1,3,5-trimethyladamantylammonium ion, both organics being incorporated into the structure. A boron analog of MCM-22 (ERB-1) has also been synthesized (6). All these zeolites share the MWW structure (7).

While an important number of diffusion and catalytic applications of the MCM-22 (8–10) and MCM-36 (11, 12) zeolites has been published, as well as modifications in the synthesis procedure (13), little is known about the properties of other members of the MWW family such as MCM-56 and MCM-49. Indeed, a novel MWW-type zeolite, named MCM-56 (14), has been synthesized which exhibits some similarities with other zeolites such as MCM-22 and MCM-49 (15). MCM-56 can be thermally treated without affecting its layered structure in that it can still be swelled after thermal treatment (14). It has been presented in the patent literature that the most interesting feature of MCM-56 in comparison with MCM-22 is that while the former adsorbs somewhat less *n*-hexane and 2,2-dimethylbutane than MCM-22, it adsorbs larger amounts of a more bulky molecule such as 1,3,5-trimethylbenzene (TMB), and also shows a much faster rate of adsorption of 2,2-dimethylbutane than MCM-22. These results seem indicate that a larger portion of "external surface" is exposed in the case of MCM-56.

Recently a new material named ITQ-2 (16) has been prepared by swelling and delaminating a MWW precursor. In this way a solid formed by very thin sheets (approximately 2.5 nm high) with an extremely high external surface area ($\geq$700 $m^2\ g^{-1}$) was produced. These sheets consist of an hexagonal array of "cups" that penetrate into the sheet from both sides. These cups would have an aperture of approximately 0.7 nm, formed by a 12-member ring (MR). The cups, which are 0.7 nm deep meet at the center of the layer forming a double 6-MR window that connects the cups, bottom to bottom. As a result, a smooth 10-MR channel system runs around the cups, inside the sheet.

In the present work, a sample of MCM-56 has been synthesized following the procedure outlined in reference (14),

[1] To whom correspondance should be addressed.

0021-9517/00 $35.00

and compared with MCM-22 and ITQ-2 samples. The textural properties of these materials have been extensively investigated by adsorption of different molecules. IR spectroscopy of adsorbed pyridine and 2,6-ditertbutyl pyridine (DTBPy) has allowed us to distinguish between acid sites in 10 MR micropores and on the "external" surface. In addition XRD and ^{29}Si MAS NMR have been used to discuss the short- and long-range structural order. Finally catalytic experiments have been carried out using reactants with different molecular sizes, and the activity associated with active sites accessible through the micropores and through the external surface has been compared for MCM-22, MCM-56, and ITQ-2.

EXPERIMENTAL

Materials

MCM-56 was prepared by following the recipe described in example 1 of U.S. patent 5,362,697 (14). Thus, 3 g of NaOH (Merck) was dissolved in 268 g deminarelized water while stirring. To this solution 6.33 g sodium aluminate (Riddel-de Haën, 45 wt% Al_2O_3, 41 wt% Na_2O) was added. After all the sodium aluminate was dissolved, 57.4 g fumed silica (Hi-Sil 233-D, PPG) was introduced and a gel was formed. Finally, 27.1 g hexamethyleneimine (HMI) (Aldrich) was added to complete the synthesis gel. The final molar composition of the gel was

$$240SiO_2 : 10Al_2O_3 : 24Na_2O : 84HMI : 4490H_2O.$$

The gel was put in a stirred autoclave (Parr) and held at 143°C for 60 h while stirring at 400 rpm. The product was isolated by filtration and extensively washed with deminarelized water. The yield after drying at 120°C was about 47 g of MCM-56 with a Si/Al ratio of 9.

The layered MCM-22 (*P*) precursor was prepared using hexamethylenimine (HMI) (Aldrich), silica (Aerosil 200, Degussa), sodium aluminate (56% Al_2O_3, 37% Na_2O, Carlo Erba), sodium hydroxide (98% Prolabo), and deionized water. More specifically a sample with $Si/Al = 50$ was prepared in the following way. $NaAlO_2$ (0.234 g) and NaOH (0.816 g) were dissolved in 103.45 g of H_2O, and then 6.358 g of HMI and 7.689 g of SiO_2 were added to this solution while stirring. After 30 min of stirring the resulting gel was introduced into a 60-ml PTFE lined stainless-steel autoclave, rotated at 60 rpm, and heated at 408 K for 11 days. The chemical composition of the final gel was $SiO_2/Al_2O_3 = 100$; $OH/SiO_2 = 0.10$; $Na/SiO_2 = 0.18$. After quenching the autoclaves in cold water, the samples were centrifuged at 12,000 rpm, washed thoroughly with deionized water until a pH of <9.0 was reached, and subsequently dried at <333 K, overnight. A portion of this MCM-22 (*P*) was calcined in air at 853 K for 3 h giving MCM-22. Another portion was used to prepare the ITQ-2 sample by swelling the precursor with hexadecyltrimethyl-ammonium bromide. Typically, 27 g of precursor was mixed with 105 g of an aqueous solution of 29 wt% surfactant and 33 g of an aqueous solution of 40 wt% tetrapropylammonium hydroxide and refluxed for 16 h at 353 K. The completion of swelling can be monitored by X-ray diffraction, which shows an increase in the distance between the layers from 2.7 nm to approximately 4.5 nm. The layers are forced apart by placing the slurry in an ultrasound bath (50 W, 40 kHz) for 1 h. Subsequent addition of a few drops of concentrated hydrochloric acid, until the pH is below 2, allows harvesting of the solids by centrifuging. Then, removal of the organic material by calcination at 813 K yields ITQ-2.

Methods

Adsorption of TMB was carried out with a volumetric apparatus coupled with a heat-flow microcalorimeter of the Tian-Calvet type (BT, Setaram). Before the hydrocarbon admission the samples were heated *in situ* up to 723 K in a flow of O_2 (30 cc min^{-1}) and kept at this temperature for 2 h. Adsorption was extended up to the maximum feasible pressure for the adsorbate, restricted by its vapor pressure and the temperature of the dosing zone of the apparatus. Amount adsorbed is expressed as millimoles per gram of sample dried under vacuum at 723 K.

^{29}Si MAS NMR spectra were recorded using a Varian VXR 400 SWB spectrometer with a 5-μs pulse corresponding to a flip angle of 45° and a 40-s repetition time. Between 1000 and 2000 scans were accumulated for each spectrum and chemical shifts were reported relative to TMS.

IR spectra were obtained in a Nicolet 710 FTIR. spectrometer (4 cm^{-1} resolution) while N_2 and Ar adsorption/desorption isotherms were performed at 77 and 87.3 K, respectively, in an ASAP 2010 apparatus from Micromeritics, after pretreating the samples under vacuum at 673 K overnight.

Acidity measurements were carried out by adsorption/desorption of pyridine followed by IR spectroscopy. Self-supported waters (10 mg cm^{-2}) of calcined samples, previously activated at 673 K and 10^{-2} Pa overnight in a Pyrex vacuum cell, were contacted with 6.5×10^2 Pa of pyridine vapor at room temperature and desorbed in vacuum at increasing temperatures (423, 523, and 623 K). The spectra were recorded at room temperature. All the spectra were scaled according to the sample weight. Adsorption coefficients calculated by Emeis (17) were used. Analogous experiments but using DTBPy (18) as probe molecule were also carried out.

Catalytic Experiments

1,3,5-Triisopropylbenzene (TIPB) and *n*-decane were cracked in an automated microactivity test unit at 773 K, at catalyst-to-oil ratios from 0.3 to 0.8 g g^{-1}. Amounts 0.200

and 0.500 g of catalyst were used for the cracking of TIPB and *n*-decane, respectively. Cyclic experiments involved the following: (a) strip the catalyst with N_2 for 20 min followed by reaction for 20 and 60 s time on stream, (b) strip with N_2 at reaction temperature (20 min, 30 ml min^{-1}), and (c) regenerate the catalyst at 793 K for 3 h with an air flow of 80 ml min^{-1}. The liquid fraction of the product was analyzed by gas chromatography and mass spectroscopy. The gaseous products were analyzed by gas chromatography. The solid products (coke) deposited on the catalyst during the reaction were quantified measuring the CO_2 produced during regeneration with an on line IR detector. Only experiments with mass balances ≥95% were considered. Kinetic rate constants were obtained by fitting the conversion data at different contact times to a first order kinetic rate equation.

RESULTS AND DISCUSSION

X-Ray Diffraction

The X-ray diffraction (XRD) patterns (Cu$K\alpha$ radiation) of the MCM-22 and MCM-56 calcined samples are given in Fig. 1. The samples can be differentiated in the region of 8.8–11.2 Å *d*-spacing where MCM-22 exhibits two resolved maxima at ~8.8–9.2 and 10.8–11.2 Å, with a distinct depression between them, while MCM-56 is characterized by two broad bands centered around 9.9 and 11 Å *d*-spacing. More specifically, it can be said that all peaks corresponding to Miller's indexes (*hk*0), i.e., those in which the *c* axis does not intervene, are essentially the same in MCM-22 and MCM-56 (see Figs. 1a and 1b). On the other hand, all peaks in which the *c* axis contributes (*hkl*) either decrease or become broader. It appears, then, that the MCM-56 structure is, with respect to MCM-22, disordered along the *c* axis and this disorder is preserved after calcination. However, it is clear that MCM-56 does not correspond to a delaminated material, as is the case of ITQ-2 (Fig. 1d), since the intensity of the diffraction peaks are maintained in the former.

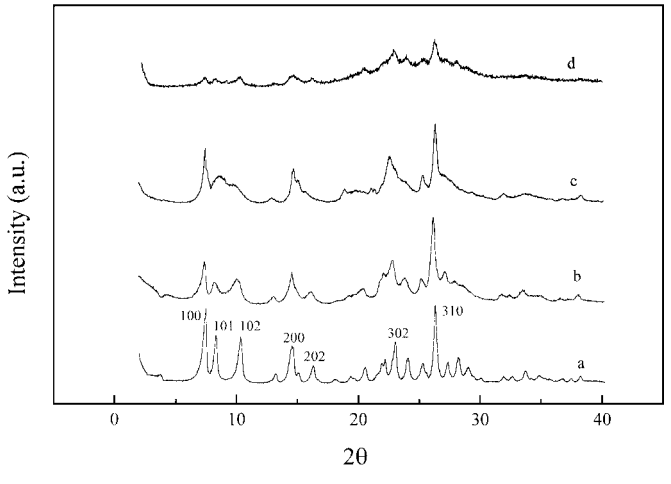

FIG. 1. X-ray diffraction patterns of MCM-22 (a), MCM-56 (b), MCM-22 precursor treated with acetone (c), and ITQ-2 (d).

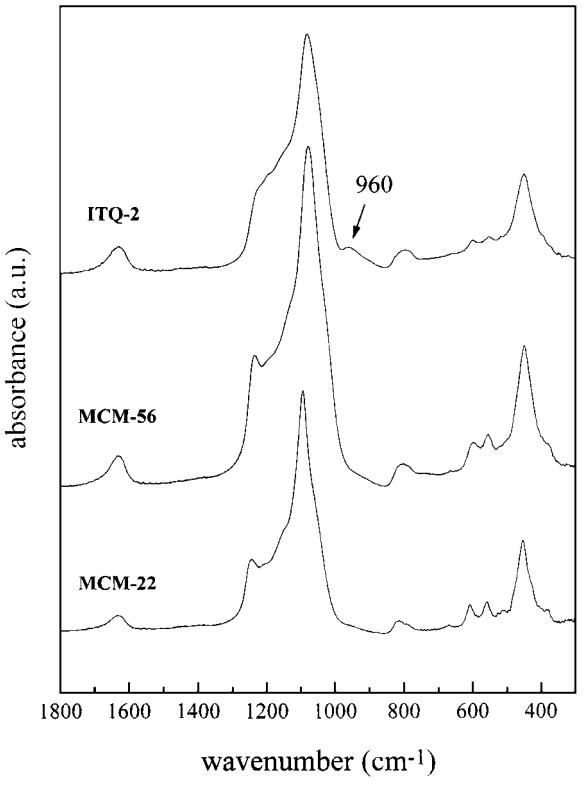

FIG. 2. Infrared spectra, in the framework region, of MCM-22, MCM-56, and ITQ-2.

In order to prove that the XRD differences between MCM-22 and MCM-56 are due only to certain disorder along the *c* axis, we have taken the laminar precursor of MCM-22 and we have treated this with acetone which can be intercalated between the layers, producing disorder along the *c* axis. After doing this the XRD pattern of the resultant material (see Fig. 1c) looks very similar to that of MCM-56 (see Fig. 1b and Ref. 14). The diffractograms still look identical after calcining the acetone-containing sample.

The XRD pattern of ITQ-2 (Fig. 1d) shows a general decrease in intensity and a broadening of the peaks consistent with the proposed structure of exfoliated layers oriented randomly (16). In contrast, we think that in MCM-56 the layers are stacked in a face-to-face orientation but disordered along the *c* axis and exhibit the characteristic 2.5-nm periodicity typical of the MWW topology.

The above conclusions are consistent with the IR results in the framework vibration region. Indeed (see Fig. 2), the band at ~960 cm^{-1} characteristic of the presence of ≡SiOH terminal groups is absent in MCM-22 and MCM-56, while it is clearly visible in ITQ-2, again indicating that no

TABLE 1

Textural Characteristics

Sample	S_{Tot} (BET)	$S_{ext.}$ (t plot)	S_{micro}[a]
MCM-22	453	111	342
MCM-56	400	156	244
ITQ-2	840	790	50

[a] S_{micro} was calculated as the difference between S_{Tot} and S_{ext}.

delamination occurred during the synthesis and activation of MCM-56.

N_2 and Ar Adsorption

The BET surface area of the calcined MCM-56 is 400 m^2 g^{-1}, which is approximately the same as for MCM-22 and one-half of that of ITQ-2 (Table 1). Moreover, in MCM-56 only 156 m^2 g^{-1} corresponds to meso and/or external surface area. This, nevertheless, is larger than in the case of MCM-22, (111 m^2 g^{-1}) but it is far from the value of the ITQ-2 sample.

The shape of the N_2 adsorption–desorption isotherm is also quite useful to discuss the textural characteristics of the various materials. The isotherms of MCM-56 and MCM-22 are very similar, showing a marked hysteresis at high p/p_0 values, indicating that the crystal sizes are small and they present a relatively high external surface area with little mesoporosity (see Fig. 3a). On the other hand, the hysteresis cycle for the ITQ-2 ends up at very low p/p_0 values (~0.4), indicating the presence of mesopores. Moreover the isotherm for ITQ-2 shows an important increase of the adsorption at p/p_0 between 0.3 and 0.4 which corresponds to mesoporosity and which is absent in MCM-56 and MCM-22. These results indicate that, from a textural point of view MCM-56 is much closer to MCM-22 than to ITQ-2. A further confirmation of this conclusion has been achieved from the Ar isotherms. Indeed, results from Fig. 3b clearly show that all the three samples have a system of pores which starts to fill up at $p/p_0 \cong 5 \times 10^{-6}$. A second inflection point in the isotherm at a p/p_0 of $\sim 5 \times 10^{-3}$ is present in MCM-22 and MCM-56 but is absent in ITQ-2. Since the first inflexion point corresponds to the filling of 10-MR micropores while the second one is assigned to the filling of 12MR pores, we can conclude that the 12-MR supercages have disappeared only in ITQ-2, while supercages remain in MCM-56 and MCM-22. In the case of ITQ-2, these supercages will disappear, giving like an external surface behavior if the layers were taken apart, being the delamination the limiting situation. Moreover, the very large external surface area of ITQ-2 also indicates that some of the layers have been

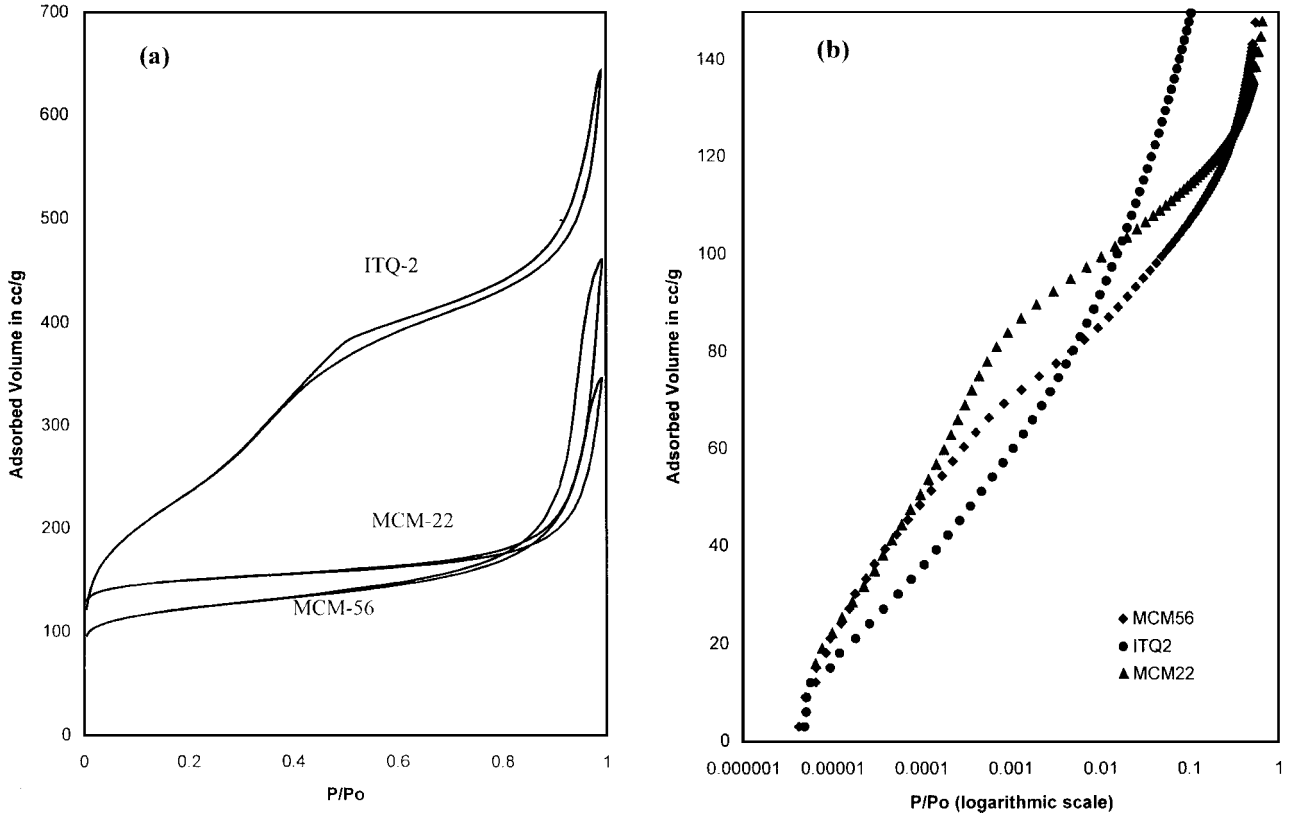

FIG. 3. Nitrogen (a) and argon (b) adsorption isotherms of MCM-22, MCM-56, and ITQ-2.

TABLE 2

Adsorption of 1,3,5-Trimethylbenzene

Sample	T (K)	p/p_0	mmol g^{-1}
MCM-22	315	0.053	0.14
MCM-56	315	0.065	0.17
ITQ-2	315	0.078	1.00

broken given smaller plates sizes in the $x+y$ dimension.

Hydrocarbon Adsorption

A further insight into the pore structure of these three materials has been gained through the adsorption–microcalorimetric study of TMB. Following the methodology described previously (19), the adsorption capacity of the three samples for TMB which cannot penetrate through 10-MR windows and therefore can be adsorbed only on the external surface (external cups) are given in Table 2. These values have been determined at the inflection point in the curve of heat of adsorption vs amount adsorbed that corresponds to the adsorption on the mesopore surface (19).

The results show that MCM-56 adsorbs some 25% more TMB than MCM-22, indicating that the external surface area of the former is larger. However, the adsorption capacity of ITQ-2 is much higher than that of MCM-22 or MCM-56. This is in agreement with the much larger external surface area of ITQ-2 (a much larger number of external cups) as a consequence of the delamination produced during the formation of ITQ-2.

^{29}Si MAS NMR

The ^{29}Si MAS NMR spectra (Fig. 4) indicate, once again, the high structural similarity between MCM-22 and MCM-56, and their differences with ITQ-2. Both MCM-22 and MCM-56 show an intense peak at −119 ppm (Si (4Si)) and −98 ppm (Si (1Al 3Si) and Si (1OH 3Si)), which indicate that in MCM-22 and MCM-56, the long-range structural order is maintained. However, in the case of ITQ-2, a broadening of the spectra, as well as a clear decrease in the −119 ppm band is observed, while the population of ≡Si–OH (−98 ppm) and $=Si(OH)_2$ (∼−92 ppm) strongly increases as a consequence of the delamination process.

Infrared and Acidity Measurements

The IR spectra (hydroxyl region) of the three materials show (Fig. 5) the presence of a hydroxyl band at 3623 cm^{-1} which correspond to bridging hydroxyl groups that are acidic and accessible to the pyridine. Moreover, and in the case of the MCM-56, a hydroxyl band at 3668 cm^{-1} that does not interact with pyridine and therefore can be associated to hydroxylated extraframework Al species is clearly visible. The ^{27}Al MAS NMR spectra (spectra not shown)

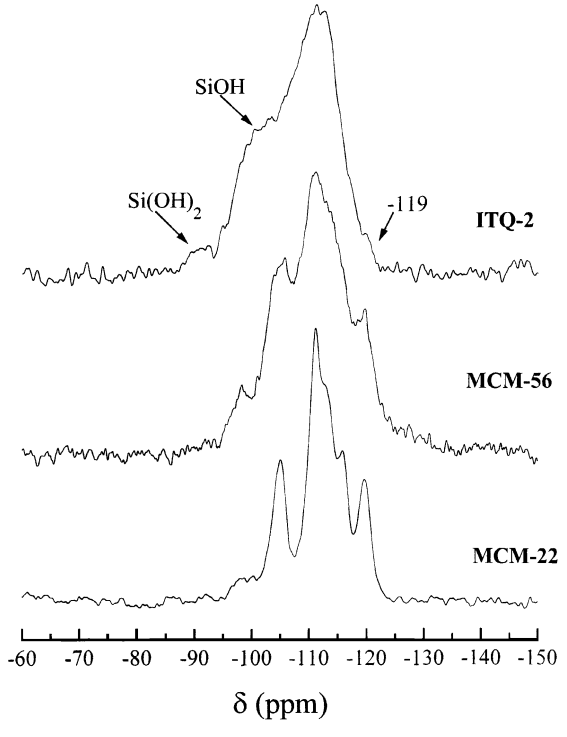

FIG. 4. ^{29}Si MAS NMR spectra of MCM-22, MCM-56, and ITQ-2.

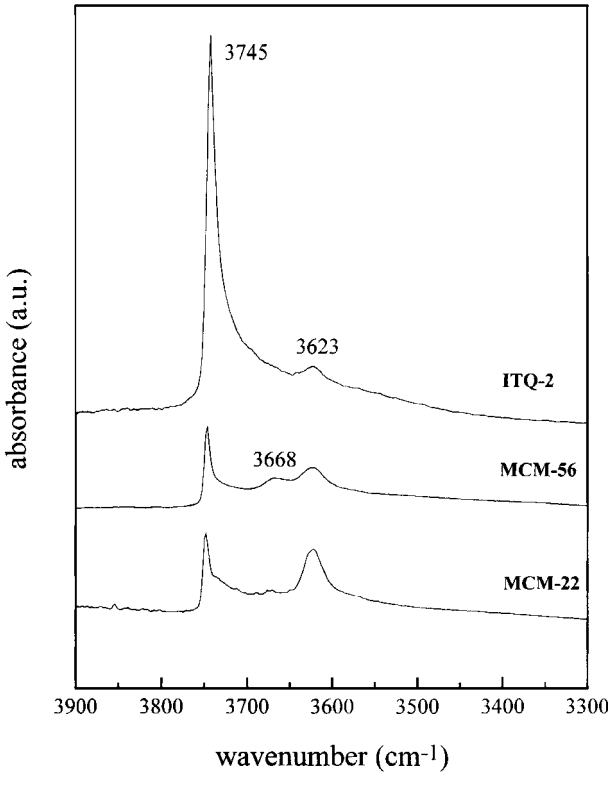

FIG. 5. Infrared spectra, in the hydroxyl stretching region, of MCM-22, MCM-56, and ITQ-2.

TABLE 3

Pyridine Adsorption at Different Temperatures

Sample	Brønsted			Lewis		
	423 K	523 K	573 K	423 K	532 K	573 K
MCM-22	57	48	33	23	20	20
MCM-56	64	59	35	77[a]	25	21
ITQ-2	21	15	9	23	20	15

Note. Values are in μm mol · py/g of zeolite.

[a] Pyridine adsorbed simultaneously on extraframework aluminum and sodium ions.

clearly show a signal at ~0 ppm, which is more intense in the MCM-56 and supports the formation of extraframework aluminum (EFAL) species during the thermal treatment. Taking this into account, it appears then that the amount of EFAL formed is larger for the MCM-56 sample which started with a lower framework Si/Al ratio.

The band associated with pyridine coordinated to Lewis acid sites (~1455 cm^{-1}) also shows the presence of extraframework Al species in all samples and, in general, its intensity follows the order MCM-56 > MCM-22 > ITQ-2 in agreement with the Al content of the starting samples (see Table 3). The intensity of the pyridine band associated to the presence of Brønsted sites (pyridinium ions, ~1550 cm^{-1}) also follows the order of the framework Al content of the starting samples. If one considers that pyridine can reach all the Brønsted acid sites present in the three samples, it is possible to conclude that the total number of Brønsted acid sites follows the order MCM-56 > MCM-22 > ITQ-2. It should then be expected that the catalytic activity for reactions catalyzed by Brønsted acid sites, where the reactant can easily diffuse through 10-MR windows, should follow the order MCM-56 > MCM-22 > ITQ-2. This trend was indeed observed when the cracking of a *n*-alkane (*n*-decane) was performed on the three samples (see Table 4). However, it is worth mentioning that the stability of the samples is different. For instance, when a series of cyclic experiments were carried out following the steps N_2 stripping, reaction, N_2 stripping, and calcination in air to burn off the coke deposited on the catalyst, we have observed that if we do not consider the first experiment which is necessary to equilibrate the catalyst, the catalyst activity from the second to the fourth repeated experiment decreases by 25, 8, and 5% for MCM-56, ITQ-2, and MCM-22, respectively. At present we have not a definitive explanation for this, but what may occur is that some dealumination still takes place during the regeneration of the catalyst at 550°C in the presence of the steam generated when burning the coke.

TABLE 4

Kinetic Rate Constants (s^{-1}) for Cracking *n*-Decane and TIPB on the Different Zeolite Samples

Sample	K (s^{-1}) × 10^2 *n*-decane	K (s^{-1}) × 10^2 TIPB
MCM-22	2.8	8.6
MCM-56	3.5	9.9
ITQ-2	1.9	25.1

TABLE 5

Adsorption of DTBPy

Sample	I_{3365} (u.a.)	μmol PyH^+ g^{-1}
MCM-22	2.3	57
MCM-56	3.0	64
ITQ-2	3.7	21

On the other hand, and in order to explore the number of acid sites available to molecules too large to penetrate through 10-MR windows, we have carried out the adsorption of 2,6 ditertbutyl pyridine (DTBPy) (18). This molecule can be easily protonated by Brønsted acid sites, giving an IR adsorption band for the protonated molecule at 3365 cm^{-1}. The results obtained (see Table 5) show that even if the Si/Al ratio of ITQ-2 is higher than those of MCM-22 and MCM-56, ITQ-2 adsorbs ~20% more DTBPy than MCM-56 which in turn adsorbs some 25% more than MCM-22. This again confirms that the number of accessible acid sites is somewhat higher in MCM-56 with respect to MCM-22, but in both cases they are lower than in ITQ-2.

If this is the case, we should expect the catalytic activity for a reaction catalyzed by Brønsted acid sites which can occur only on the external surface of the crystallites (external cups) to follow the order ITQ-2 > MCM-56 > MCM-22. In order to check this, the cracking of triisopropylbenzene (TIPB) was carried out, and the results given in Table 4 show that the activity of ITQ-2 is the highest followed by MCM-56 and MCM-22.

CONCLUSIONS

From the physicochemical characterization results it appears that MCM-56 and MCM-22 are similar materials, and that they both are quite different from ITQ-2. Adsorption experiments also show a closer similarity between MCM-56 and MCM-22, their behavior being qualitatively and quantitatively different from that of ITQ-2. It appears that MCM-56 has a somewhat larger external surface area than MCM-22 as measured by N_2 adsorption, and it is also able to adsorb some 15–20% more TMB than MCM-22. This hydrocarbon can be adsorbed only at the external surface (external cups) of the structure. This is a consequence of the higher degree of disorder along the *c* axis in MCM-56 with respect to MCM-22. A similar type of disorder was observed after adsorbing acetone on the laminar precursor of MCM-22,

yielding then the same XRD as that reported for MCM-56. On the other hand, ITQ-2 has a much larger external surface area and is able to adsorb ~7 times more TMB then MCM-22 and 5–6 times more than the MCM-56 sample prepared in this work. From IR and NMR it appears that ITQ-2 has an excess Si OH relative to the ideal structure (single plates). This can be explained not only by considering that a fraction of the structure has been destroyed but it can also be an indication that ITQ-2 has some plates with smaller sizes.

The total number of Brønsted acid sites follows the same order as the framework Si/Al ratio, but the total number of the acid sites accessible through the external surface to a large probe molecule such as 26 DTBPy is highest for ITQ-2, followed by MCM-56 and MCM-22. These observations correlate well with the catalytic activity for processing a large molecule which cannot diffuse within the micropores and can react only at the external surface (external cups).

ACKNOWLEDGMENTS

We thank the Spanish CICYT for financial support (Project MAT97-1016-C02-01 and Project MAT97-1207-C03-01).

REFERENCES

1. Rubin, M. K., and Chu, P., U.S. patent 4,954,325, 1990.
2. Leonowicz, M. E., Lawton, J. A., Lawton, S. L., and Rubin, M. K., *Science* **264**, 1910 (1994).
3. Puppe, L., and Weisser, J., U.S. patent 4,439,409, 1984.
4. Zones, S. I., U.S. patent 4,665,110, 1987.
5. Camblor, M. A., Corell, C., Corma, A., Diaz-Cabañas, M. J., Nicolopoulos, S., Gonzalez-Calbet, J. M., and Vallet-Regí, *Chem. Mater.* **8**, 2415 (1996).
6. Millini, R., Perego, G., Parker, W. O., Bellusi, G., and Carluccio, L., *Microporous Mater.* **4**, 221 (1995).
7. Njo, S. L., Van Koningsveld, H., Van der Graaf, B., Baerlocher, Ch., and McCusker, L. B., "*Proceedings 12th International Zeological Conference*," Baltimore, IV, 2519. 1999.
8. Kresge, C. T., Le, Q. N., Roth, W. J., and Thompson, R. T., U.S. patent 5,258,566, 1993; Chu, P., Landis, M. E., and Le, Q. N., U.S. patent 5,334,795, 1994.
9. Perego, C., Amarilli, S., Millini, R., Bellusi, G., Girotti, G., and Terzoni, G., *Microporous Mater.* **6**, 395 (1996).
10. Sastre, G., Catlow, C. R. A., and Corma, A., *J. Phys. Chem. B* **103**, 5187 (1999).
11. Chu, C. T.-W., Kresge, C. T., Roth, W. J., Simmons, K. G., and Vartuli, J. C., U.S. patent 5,292,698, 1994; and Kresge, C. T., Roth, W. J., Simmons, K. G., and Vartuli, J. C., U.S. patent 5,229,341, 1993.
12. Roth, W. J., Kresge, C. T., Vartuli, J. C., Leonowicz, M. E., Fung, A. S., and McCullen, S. B., *in* "Catalysis by Microporous Materials" (H. K. Beyer, H. G. Karge, I. Kiricsi, and J. B. Nagy, Eds.), p. 301. Elsevier, Amsterdam, 1995; He, Y. J., Nivarthy, G. S., Eder, F., Seshan, K., and Lercher, J. A., *Microporous and Mesoporous Mater.* **25**, 207 (1998); and Corma, A., Fornés, V., Martínez-Triguero, J., and Pergher, S. B., *J. Catal.* **186**, 57 (1999).
13. Mochida, I., Eguchi, S., Hironaka, M., Nagao Sh., Sakanishi, K., and Witherhurst, D. D., *Zeolites* **18**, 142 (1997).
14. Fung, A. S., Lawton, S. L., and Roth, W. J., U.S. patent 5,362,697, 1994.
15. Lawton, S. L., Fung, A. S., Kennedy, G. J., Alemany, L. B., Chang, C. D., Hatzikos, G. H., Lissy, D. N., Rubin, M. K., Timken, H. K. C., Stenernagel, S., and Woessner, D. E., *J. Phys. Chem.* **100**, 3788 (1996).
16. Corma, A., Fornes, V., Pergher, S., Maesen, Th. L. M., and Buglass, J. G., *Nature* **396**, 353 (1998).
17. Emeis, C. A., *J. Catal.* **141**, 347 (1993).
18. Corma, A., Fornes, V., Forni, L., Márquez, F., Martínez-Triguero, J., and Moscotti, D., *J. Catal.* **179**, 451 (1998).
19. Guil, J. M., Guil-López, R., Perdigon-Melón, J. A., and Corma, A., *Microporous Mater.* **22**, 269 (1998).